

M. Roland · A. Kruglova · G. Gaiselmann ·
T. Brereton · V. Schmidt · F. Mücklich ·
S. Diebels

Numerical simulation and comparison of a real Al–Si alloy with virtually generated alloys

the date of receipt and acceptance should be inserted later

Abstract Mechanical stress–strain curves are estimated by means of numerical simulation in order to analyze and compare the mechanical properties of a real Strontium–modified Al–Si alloy with virtually designed materials. The virtual materials are generated by a competitive stochastic growth model of the 3D coral–like morphology of the eutectic Si in Al–Si alloys. The experimental data for the real material was acquired using FEB/SEM tomography. The numerical simulations are based on finite element methods. The effects of coarsening the mesh size and using different degrees of the finite elements are discussed. The simulations show that there is high conformity between the mechanical properties of the real and virtual materials. Experiments are also performed to show that the mechanical behavior of the realizations of the stochastic model is sensitive to changes in the parameters that control the morphological characteristics of the Si component.

Keywords numerical simulation of virtual materials · virtual materials design · stochastic growth model · Al–Si alloys · FIB/SEM tomography

1 Introduction

There is a steadily increasing need for light Al–Si alloys in the modern automotive industry, in which, due to their good casting properties and strength–to–weight ratio, they are replacing

M. Roland · S. Diebels
Lehrstuhl für Technische Mechanik, Universität des Saarlandes, 66123 Saarbrücken, Germany
Tel.: +49-681-302-2169
Fax: +49-681-302-3992
E-mail: m.roland@mx.uni-saarland.de, s.diebels@mx.uni-saarland.de

A. Kruglova · F. Mücklich
Lehrstuhl für Funktionswerkstoffe, Universität des Saarlandes, 66123 Saarbrücken, Germany
Tel.: +49-681-302-70500
Fax: +49-681-302-70502
E-mail: anastasia.kruglova@uni-saarland.de, muecke@matsci.uni-sb.de

G. Gaiselmann · T. Brereton · V. Schmidt
Institut für Stochastik, Universität Ulm, 89069 Ulm, Germany
Tel.: +49-731-50-23532
Fax: +49-731-50-23649
E-mail: gerd.gaiselmann@uni-ulm.de, timothy.brereton@uni-ulm.de, volker.schmidt@uni-ulm.de

heavier cast iron, which has long been used as a major component in the production of engine bodies, see (8). The improved mechanical properties of Al–Si alloys (in particular the increased tensile strength and ductility) are mostly due to the specific Si morphology obtained by using a modification treatment as explained in (3; 9; 18). The modification treatment is performed by adding small amounts of certain elements (such as Sr or Na) to the alloy. This promotes the twinning of Si particles and refines the eutectic phase. Typically, the modified Si particles solidify into coral-like or fibrous shapes as shown in (10).

It has long been established that a Sr-based modification treatment improves the mechanical properties of Al–Si alloys and it is now used regularly. However, the mechanisms leading to certain structural transformations and the relationship between the morphology and mechanical properties of modified alloys are still not understood very well. In practice, a large number of experiments must be carried out in order to identify these mechanisms and determine the relationship between the structure of a material and its mechanical properties. Such experiments, which include quantitative analyses of the microstructure and mechanical tests, are very expensive in terms of time, materials, and analyses costs. As a result, simulation techniques capable of generating virtual microstructures in the form of 3D digitized pictures are often used as a cheaper and more efficient alternative to real world experiments. The output from these models can be analyzed using a variety of numerical methods, including the finite element method (FEM). One of the most advanced techniques for creating virtual structures is stochastic modeling. In recent years, this method has attracted much attention and has been successfully applied in various areas of materials science such as organic solar cells, fuel cells, batteries, foams and glass fiber systems; see, for example, (4; 6; 19; 20; 21).

Recently, a stochastic growth model has been developed for the 3D morphology of the eutectic Si in Al–Si alloys (specifically, directionally solidified alloys); see (5). It has been shown that there is a high conformity between the morphological characteristics of realizations of this stochastic model and the morphological characteristics of the real material. In this paper, we take the next step and show that the mechanical properties of realizations of the stochastic model closely resemble the mechanical properties of the real material. We give appropriate parameters for mechanical simulations on the Al–Si eutectic structures. Using these simulations, we validate the stochastic model. Such validation is very important, as it provides strong evidence that the stochastic model is able to reproduce the key mechanical features of the real material. We can then use the validated model to further study the relationship between the microstructure of a material and its mechanical properties by generating alternative morphological scenarios using different model parameters.

In order to effectively use FEM software tools, we generate volume meshes from the FIB/SEM tomography images using a method similar to that described in (13). We demonstrate the effect of coarsening the mesh on the simulation results, mirroring the approach used in (13). We then use load curves to investigate the mechanical behavior of the real sample and its virtual counterparts. We plot the curves for different load directions and compare them to one another. We also briefly investigate the mechanical behavior of structures produced by the stochastic model using different parameter choices. We show that the mechanical behavior of realizations of the stochastic model is sensitive to parameter changes and reacts to these changes as expected.

2 Materials and Methods

The 3D morphology of the real sample was acquired using FIB/SEM tomography, as described in (7), of the eutectic region of a hypoeutectic AlSi7 alloy modified by the addition of 150 ppm of Sr. The volume contains about 200 clusters of Si (depicted with different colors in Figure 2 (left)) with a total volume fraction of about 12%. These structures are elongated in one direction due to the production process. The 3D image of the sample comprises a series of 195 plain images. The slice thickness of the image stack is constant and equals 180 nm (the distance between two

plain images). The height and width are 285 and 790 pixels, respectively. The pixel spacing of the images is $58 \text{ nm} \times 46 \text{ nm}$. The images are then rotated and rescaled to the same pixel spacing of 46 nm. The new slice thickness is then also 46 nm. Thus, all pixels are transformed to cubical voxels with an edge length of 46 nm. After the preparatory steps are performed, the image data is passed on to a finite element mesh procedure.

3 Stochastic Modeling of Eutectic Si in Al–Si Alloys

In this section, we briefly describe a competitive stochastic growth model, introduced in (5); for the simulation of 3D coral-like morphologies. A coral-like morphology consists of a system of pairwise disconnected 3D corals, in which each coral is a tree-like structure. The microstructure of the eutectic Si in modified Al–Si alloys has a coral-like morphology, as can be seen in Figure 2 (left). The model we describe is based on tools from stochastic geometry and time series analysis. Roughly speaking, coral-like morphologies are modeled as disconnected systems of dilated line segments. For reasons of brevity, we only give a brief description of the model here. A complete description of the stochastic morphology model is given in (5).

We grow the system of corals according to a dynamic procedure. In this dynamic procedure, corals ‘compete’ with one another for space. We begin by placing the ‘seeds’ of the corals randomly in the sampling window. We place these seeds in such a way that the minimum distance between two seeds always is at least r_{cox} ; see Figure 1(left).

We then grow corals from these seeds in an iterative fashion. At each step of our procedure, we add new line segments with random orientations to every coral that is still able to grow. These line segments are generated using a time series model that is fully described in (5). We check that each new line segment satisfies two criteria. The first criterion is that it cannot be too close to a line segment of another coral. That is, if one coral already occupies a certain region of space, no other coral can grow into that space. We measure their closeness by considering the Euclidean distance from the unconnected endpoint of the new line segment to the nearest point of another coral. If this distance is less than τ_{external} , we delete the new line segment and no longer add any line segments to the part of the coral from which it originated. If two new line segments are too close to one another, we delete one of them according to a rule specified in (5). Figure 1(right) shows a number of new line segments that are too close to the line segments of other corals. The second criterion is that new line segments cannot be too close to existing line segments of the same coral in the sense that the Euclidean distance from the unconnected endpoint of a new line segment to points in other line segments of the same coral must be greater than τ_{internal} . Figure 1(center) shows a number of line segments that are too close to other line segments of the same coral. If a new line segment is too close to an existing line segment, it is deleted and no new line segments are added to the part of the coral from which it originated.

This iterative process is continued until it is no longer possible to add additional line segments to any existing coral. If, after all the corals have stopped growing, there are still large regions of empty space, we put additional seeds in these regions of space and grow more corals from them. Once the line segments of the coral system have been fully generated, they are dilated in 3D. The volume of the dilated line segments is determined by the parameter $r_{\text{dil}} \geq 0$.

By varying the parameters of the stochastic model, we are able to generate random 3D morphologies with different structural properties. The most important parameters are r_{cox} , τ_{external} , τ_{internal} , and r_{dil} . Their explicit influences on the structural properties are as follows:

- r_{cox} controls the number of distinct corals and the distance between corals.
- τ_{external} determines the minimum distance between pairs of distinct corals.
- τ_{internal} controls the degree of branching and the distance between the branches of the individual corals.
- r_{dil} controls the volume fraction of Si.

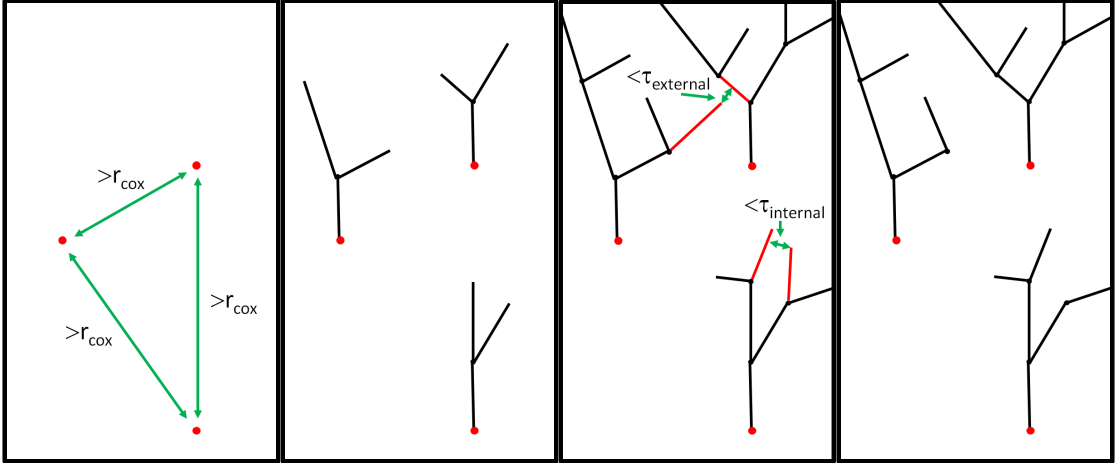


Fig. 1 Basic idea of the competitive stochastic growth model. Left: The seeds of the corals are randomly placed with a minimum distance of r_{cox} . Center left: Random line segments are added to the corals. Center right: New line segments are checked to ensure that they satisfy the two criteria. Right: Line segments that violate the criteria are deleted.

Stochastic morphology models are primarily used as tools for better understanding the relationship between the microstructure and functionality of a material. In particular, the stochastic models can be used to generate a series of virtual (but realistic) microstructures, in which morphological features that are assumed to influence the material's functionality are systematically varied. Numerical simulations can be performed on these structures to predict their functionality. The output of the numerical simulations is analyzed and evaluated to elucidate the relationship between changes in the morphological features of a material and resulting changes in its functional properties.

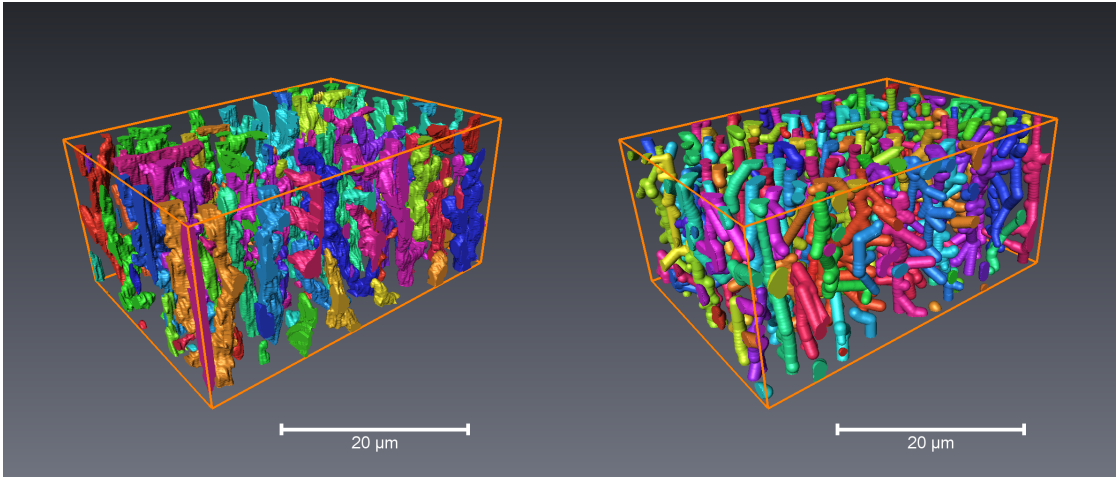


Fig. 2 3D morphology of experimental Si corals in an Al matrix (left) and a realization drawn from the fitted competitive stochastic growth model (right).

In (5), we fitted the competitive stochastic growth model to the microstructure of the eutectic Si in modified Al–Si alloys. That is, we chose the parameters of the stochastic model in order

to obtain the best possible agreement between the important structural characteristics of experimental 3D image data of the eutectic Si and the corresponding characteristics estimated from realizations of the stochastic model. The fitted parameters obtained were $\tau_{\text{internal}} = 1.38 \mu\text{m}$, $\tau_{\text{external}} = 0.92 \mu\text{m}$, $r_{\text{cox}} = 2.53 \mu\text{m}$, and $r_{\text{dil}} = 0.55 \mu\text{m}$, cf. (5).

A visual comparison of the images produced by the stochastic model with the experimental FIB/SEM image (Figure 2) suggests that the stochastic model provides a good fit to the real data. This is confirmed via formal model validation using structural characteristics (e.g. density of corals) that were not used to calibrate the stochastic model; see (5). Although the structural characteristics of the stochastic model strongly agree with the characteristics of the real data, this does not necessarily imply that the microstructures generated by the stochastic model and the experimental microstructure have similar mechanical properties. In this paper, we investigate the mechanical properties of both the eutectic Si and realizations of the fitted stochastic model. Because realizations of the stochastic model are inherently random, we consider a number of different realizations. We show that the mechanical properties of all these realizations are as expected.

As we also aim to analyze the sensitivity of mechanical properties to changes in the microstructure, we generate two further virtual microstructures. We produce these microstructures by, in each case, changing a single parameter of the fitted stochastic model. We choose the new parameter values so that the resulting stochastic models produce realizations that are significantly different to the realizations of the fitted stochastic model. In the first case (Figure 3(left)), the parameter τ_{internal} is reduced. This results in a microstructure with a small number of very large corals. In the second case, (Figure 3(right)), the parameter r_{cox} is reduced. This results in a microstructure with a large number of smaller disconnected clusters which have small pairwise distances to each other. In both cases, the resulting realizations have a larger volume fraction of the eutectic Si. Specifically, the volume fraction increases from roughly 12% (for both the real sample and the virtual samples generated using the fitted model parameters) to approximately 28%. It is well known that the mechanical properties of Al-Si are sensitive to changes in the volume fraction of Si. Thus, we can demonstrate that changing the parameters of our model still results in realistic virtual materials by showing that the realizations with a higher proportion of Si possess the expected mechanical properties. Thus, the sensitivity analysis carried out in this paper can be regarded as a plausibility check of the combination of stochastic microstructure generation with mechanical behavior simulations. In addition, although both kinds of virtual microstructures have approximately the same volume fractions, they have different clustering properties. Thus, the mechanical responses of these microstructures shed light on the effect of this morphological feature on the mechanical properties.

4 Numerical results

4.1 Finite element mesh procedure

The image data from the FIB/SEM tomography can be easily transformed into a 3D volume mesh containing the cubical voxels described in Section 2. As a legacy of the complicated segmentation process that is performed in a preprocessing step, the two components of the alloy form two completely separate phases. As a result, all of the information obtained from the FIB/SEM tomography can be linearly mapped onto the finite element mesh. Using this approach, a finite element mesh with approximately 150 million voxels is generated. This presents computational difficulties as finite element simulations on meshes with such a large number of elements can only be carried out using large high-performance clusters. Thus, in order to accelerate the computations and reduce the memory requirements, we coarsen the meshes. This coarsening is performed as a preprocessing step by means of an algorithm that uses a uniform scaling with a simple box filter of variable size with respect to the volume fractions of the particular materials and their

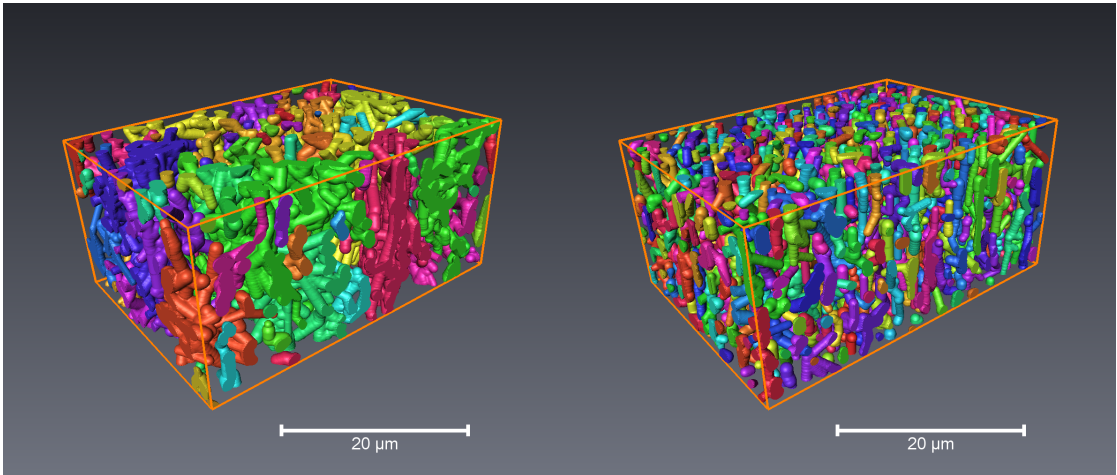


Fig. 3 Two simulations drawn from the competitive stochastic growth model with different model parameters (i.e., by reducing τ_{internal} from 1.38 to 0.46 μm (left), and reducing r_{cox} from 2.53 to 1.15 μm (right) while keeping the other parameters equal to the fitted parameters). Left: microstructure consisting of a small number of relatively large and highly interconnected clusters; right: microstructure with a large number of small and disconnected clusters.

properties. This algorithmic procedure operates on the total 3D volume mesh. In the following, the size of the box filter is called the level of the corresponding mesh and is linked to the number of voxels used for the simple filtering.

Figure 4 illustrates the effects of the coarsening of one 2D cross-section of the finite element mesh. The left image shows a cross-section of the original mesh. This comprises 550×763 pixels. The right image shows the same cross-section with a mesh produced using a coarsening level of 8. As described above, level 8 means that the box filter has a total size of $8 \times 8 \times 8$ voxels, which leads to a reduction factor of 512. It is clear from the two cross-sections that most of the structure is preserved by the coarsening operation. Only minor features of the structure are lost. In Section 4.2, we have used five different coarsened meshes. The number of mesh cells in each mesh is listed in Table 1. The coarsening algorithm was also used for all the meshes generated for the virtually designed materials as these were also 3D volume meshes.

4.2 Finite element simulations of the real Al–Si alloy sample

We used the same material properties for all the simulated Al–Si alloys and all resolutions of the mesh. For the aluminum phase, we used a Young’s modulus of $E = 70$ GPa, a Poisson ratio of $\nu = 0.34$, and a yield strength of $\sigma_y = 40$ MPa. For the silicon, we used a Young’s modulus of $E = 107$ GPa, a Poisson ratio of $\nu = 0.27$, and a yield strength of $\sigma_y = 7$ GPa.

The numerical simulations were performed using COMSOL Multiphysics. We used the structural mechanics module with an elasto–plastic material model combined with an isotropic hardening (1; 11). The isotropic tangent modulus in this model was set to $E_{Tiso} = 2.0e10$ Pa. All presented finite element simulations were done with quadratic Lagrange elements, except a few numerical tests presented in Figure 5. The corresponding number of degrees of freedom (d.o.f.) for the different tested coarsened meshes are listed in Table 1. In addition, the table also shows the computing time in seconds for the simulations on the individual meshes.

All simulations were executed on a DELL PowerEdge with two Intel Xeon CPUs and 72GB RAM. The linear systems were solved with the Flexible variant of the Generalized Minimum RESidual (FGMRES) method introduced in (14; 15) with a geometric multigrid preconditioner

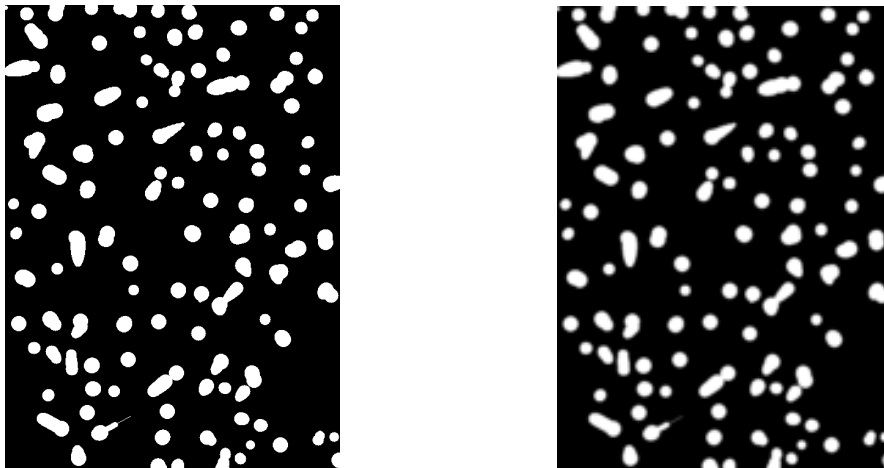


Fig. 4 One cross-section of the finite element mesh without coarsening (left) and the same cross-section for the level 8 finite element mesh (right).

with a V-cycle with two iterations, two levels, and the mesh coarsening factor two, cf. (12). The presmoothener was the Successive Over-Relaxation (SOR) method with two iterations and the relaxation factor $\omega = 1.2$ (2). The SORU method (a version of SOR using the upper triangle of the matrix, cf. (1)) was used as a postsmoother, again using two iterations and the relaxation factor $\omega = 1.0$, cf. (12). The coarse solver was the PARDISO method: a parallel sparse direct solver explained in (16; 17).

	level 8	level 9	level 10	level 11	level 12
mesh cells	284,240	199,836	146,300	110,400	82,215
d.o.f.	6,986,589	4,926,519	3,617,379	2,737,605	2,045,589
computing time	13,070 s	9,465 s	7,667 s	4,167 s	3,370 s

Table 1 List of all coarsening levels, the total number of mesh cells, the corresponding number of degrees of freedom, and the computing time for the finite element simulation.

The numerical simulations of the deformation of the Al-Si alloys were performed using the following boundary conditions: for every spatial direction, we fixed the displacement on one side of the meshes and applied a load curve to the opposite side. The boundary conditions were unloaded on the other four sides. The load curve results from the average stress and is computed based on the average displacement of the surface points. After every simulation run, we computed a stress-strain curve using numerical integration of the displacement field in the corresponding spatial direction.

Figure 5 shows several stress-strain curves for computations on the level 12 mesh. In these first numerical tests, we compare linear and quadratic finite elements for different resolutions of the load curve, i.e. numbers of load steps. One can see that the curves of the quadratic finite elements lie a little bit below the curves of the linear finite elements. The resolution of the load curve has no visible influence on the plotted results. Nevertheless, in simulations with a pure aluminum specimen instead of an Al-Si alloy, we are able to observe unphysical spurious oscillations which are in the stress-strain curve for load curves with a resolution less than 30 load

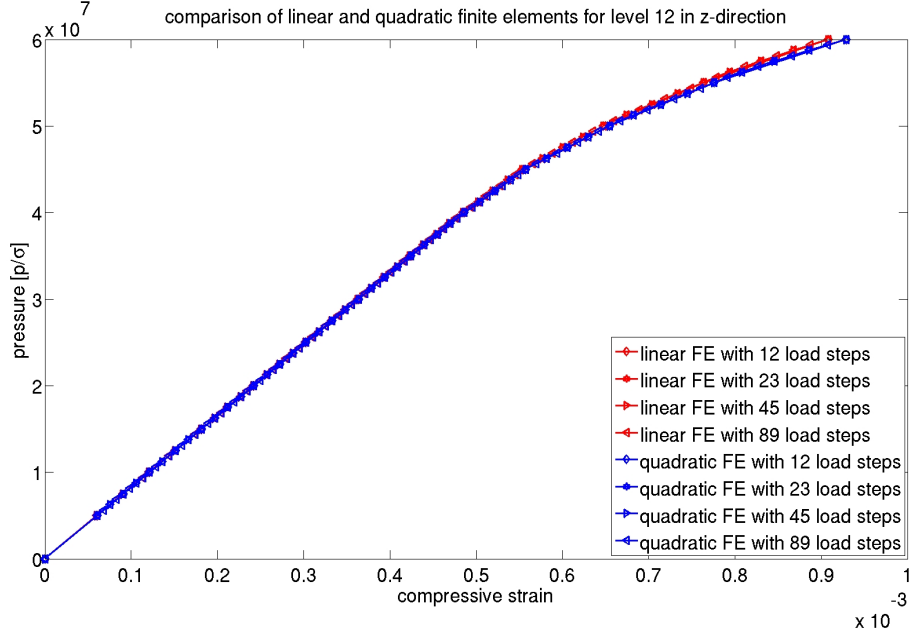


Fig. 5 Finite element simulations with linear (red) and quadratic finite elements (blue), and different numbers of load steps.

steps, caused by the used numerical methods. For this reason, we decided to use a minimum of 35 load steps in all simulations described here.

In order to show that load curves obtained by the FEM simulations quickly converge to fixed values, even for reasonably high degrees of coarsening, we compare simulations on meshes with different levels of coarsening. Figures 6 and 7 show stress–strain curves for meshes with coarsening levels from 8 to 12. The curves all have the same qualitative behavior, although the curves become straighter as the coarsening level increases. Considering the fact that x is the direction of the solidification of the eutectic Si, and y is the perpendicular direction, the convergence is independent of the orientation of the directional solidification. For more details on this kind of finite element simulations, we refer to (13), which such results are presented and discussed for Al–Si alloys with and without a directional solidification, and for different resolutions of the FIB/SEM tomography data. Because the load curves quickly converge to fixed values and because our computer power is limited, we chose to do the simulations at the coarsening level of 8.

Figure 8 shows that the stress–strain curve for a load curve in the direction of the solidification is steeper than for the other two spatial directions, for which the curves show a very similar behavior. In other words, the material shows, as expected, a transverse isotropic behavior in the y - and the z - direction, with a higher strength in the direction of the coral growth and a lower one in the transversal direction.

4.3 Finite element simulations of the virtually generated Al–Si alloys

The numerical simulations of the virtually generated Al–Si alloys were performed with the same parameters as used for the real Al–Si alloy sample. These include the material properties assumed in Section 4.2.

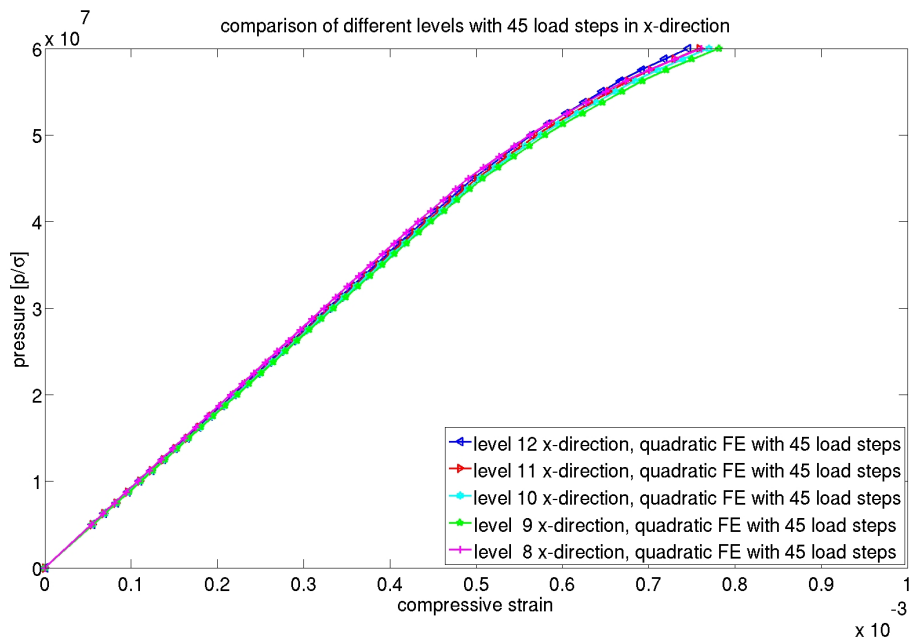


Fig. 6 Finite element simulations with quadratic finite elements in the direction of the directional solidification for different levels of coarsening.

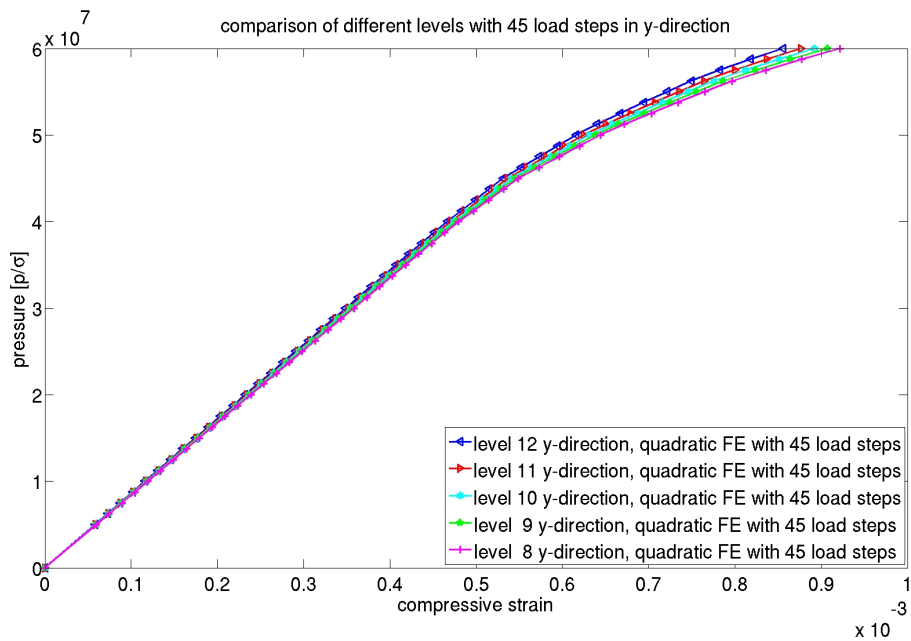


Fig. 7 Finite element simulations with quadratic finite elements perpendicular to the direction of the directional solidification for different levels of coarsening.

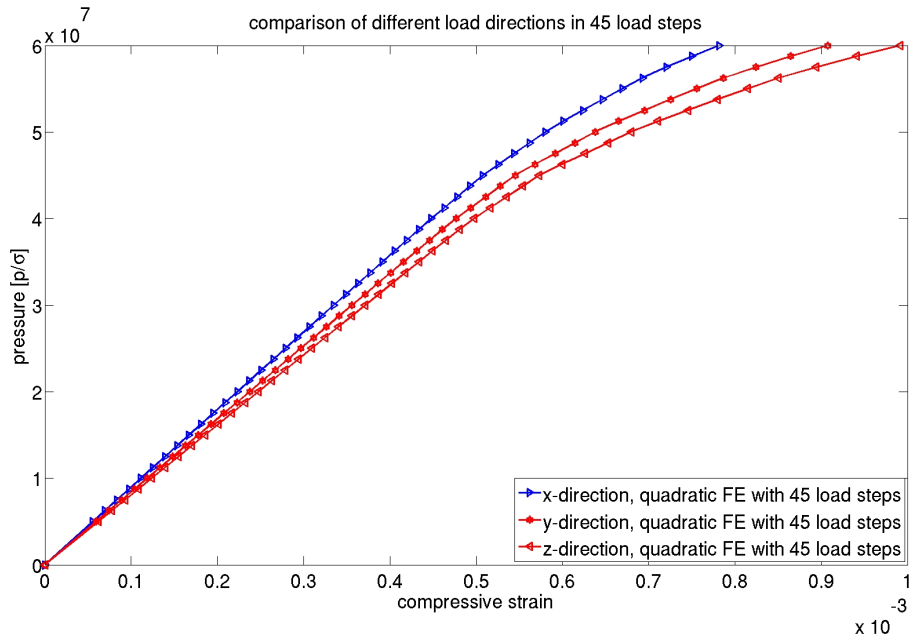


Fig. 8 Finite element simulations with quadratic finite elements for load curves in all three spatial directions.

In order to perform these simulations, we generated a series of ten morphologies using the stochastic model with the parameters fitted to the real eutectic Si in the Sr-based modified Al-Si alloy. Figure 9 shows the stress-strain curves for the real sample and the ten virtual microstructures. All of the curves show the same behavior in the elastic region. However, the curves differ, as expected, in the plastic region. The upper and lower bounds of these different curves can be interpreted as a rough confidence band with the original data nearly in the middle. In Figures 6 and 7, it is shown that the FEM simulations based on the real sample tend to converge quickly as the coarsening level of the mesh becomes smaller. This is also the case for the simulations on the virtually designed microstructures. The results given here provide strong evidence that the competitive stochastic growth model captures the essential microstructure elements of Al-Si alloys and thus is a good model for virtual materials design.

To demonstrate the sensitivity of mechanical properties to changes in the microstructure, we have carried out two simulations of virtual microstructures that have qualitatively different structures. These are also significantly different to the real microstructure. These simulations are shown in Figure 10, in which they are labeled microstructure type 2 and microstructure type 3. Microstructure type 2 has larger clusters formed by interconnected corals than the real sample. In contrast, microstructure type 3 has a larger number of smaller disconnected clusters. These have smaller pairwise distances to each other than the clusters in the real sample.

Figure 10 compares the results for these two morphologies with the results for the real sample and a virtual microstructure, called type 1, which was generated by the stochastic model using the parameters fitted to the real sample. It can be seen that the two non-physical microstructures have a higher strength than the real sample because of their higher Si volume fraction. Microstructure type 3 has a higher strength than microstructure type 2, although they both have approximately the same volume fraction of Si.

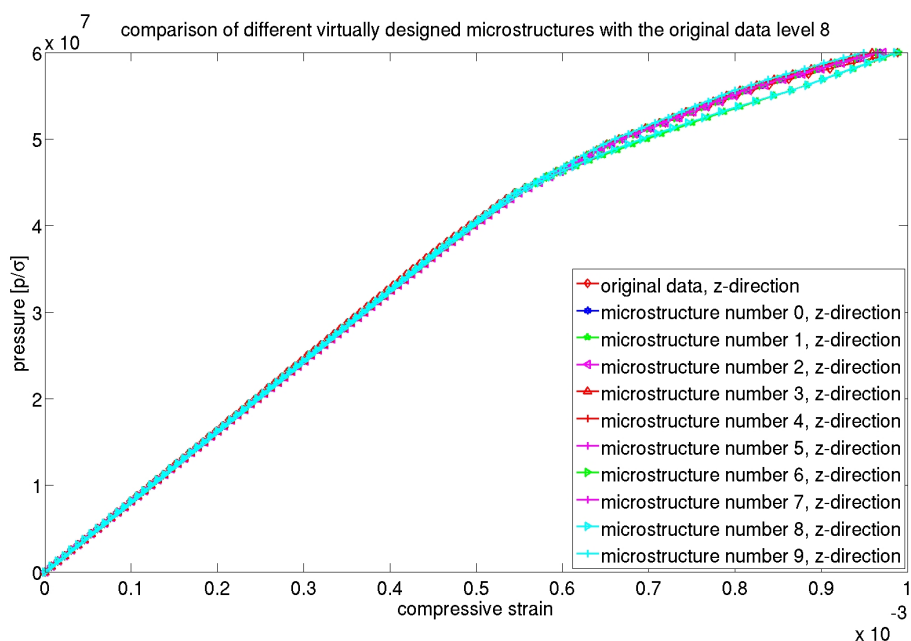


Fig. 9 Finite element simulations of ten virtually designed microstructures which are stochastically identical to the model fitted to the real sample and the original data.

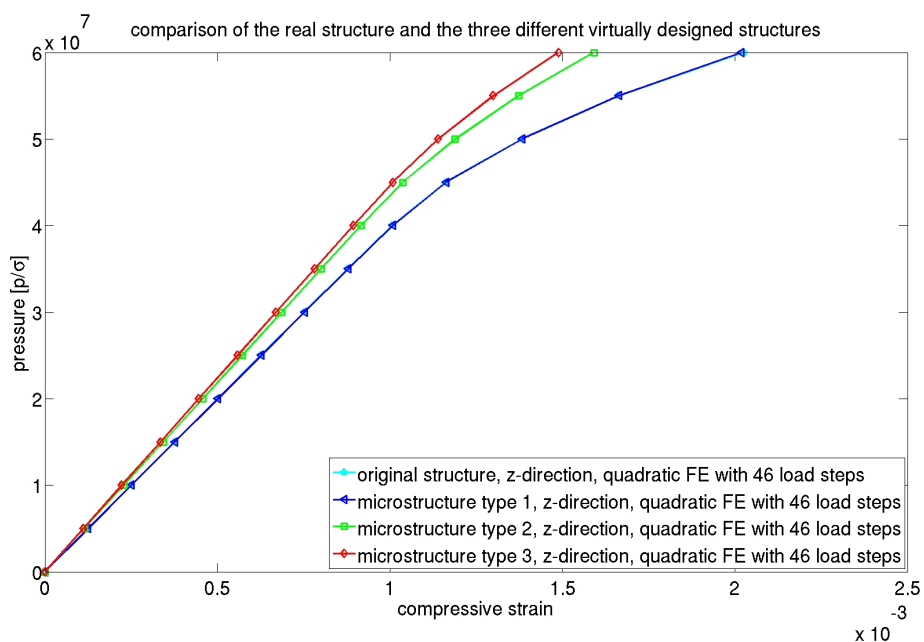


Fig. 10 Finite element simulations of the real sample, one microstructure stochastically fitted to the real sample and two microstructures with significant changes compared to the real sample.

5 Conclusions

We have generated finite element meshes with different coarsening levels directly from FIB/SEM tomography image data and from virtually designed microstructures. We have shown that the simulation results seem to converge to the correct values for reasonably high levels of coarsening, which suggests that such coarsening may be useful for making meshes that are computable with finite elements outside large high-performance clusters. We have also shown that the virtual microstructures generated by the stochastic model fitted to the real sample provide similar numerical results compared to those for the real material. By changing the parameters of the stochastic model, we are able to obtain different morphological features in the virtual materials. The numerical simulations performed on these new virtual materials give results in accord with our expectations. This suggests that the stochastic model could be a good tool for the virtual design of the eutectic Si in Sr-modified Al-Si alloys, as it generates virtual materials with mechanical properties that are consistent with those found in real materials.

Acknowledgements The financial support of the Deutsche Forschungsgemeinschaft (DFG) under the grant DI 430/17-1 is gratefully acknowledged.

References

1. COMSOL Multiphysics User's Guide. COMSOL – Version 4.1 (2010)
2. Braess, D.: Finite Elemente. Springer, Berlin (2003)
3. Closset, B., Gruzleski, J.: Structure and properties of hypoeutectic Al-Si-Mg alloys modified with pure strontium. *Metall. Trans. A* **13**, 945–951 (1982)
4. Gaiselmann, G., Neumann, M., Holzer, L., Hocker, T., Prestat, M., Schmidt, V.: Stochastic 3D modeling of LSC cathodes based on structural segmentation of FIB-SEM images. *Computational Materials Science* **67**, 48–62 (2013)
5. Gaiselmann, G., Stenzel, O., Kruglova, A., Muecklich, F., Schmidt, V.: Competitive stochastic growth model for the 3D morphology of eutectic Si in Al-Si alloys. *Computational Materials Science* **69**, 289–298 (2013)
6. Gaiselmann, G., Thiedmann, R., Manke, I., Lehnert, W., Schmidt, V.: Stochastic 3D modeling of fiber-based materials. *Computational Materials Science* **59**, 75–86 (2012)
7. Giannuzzi, L., Stevie, F.: Introduction to Focused Ion Beams. Springer, New York (2005)
8. Gruzleski, J., Closset, B.: The Treatment of Liquid Aluminum-Silicon Alloys. American Foundrymen's Society, Inc., Des Plaines, Illinois (1990)
9. Haque, M.: Effects of strontium on the structure and properties of aluminium-silicon alloys. *J. Mater. Proc. Technol.* **55**, 193–198 (1995)
10. Hegde, S., Prabhu, K.: Modification of eutectic silicon in Al-Si alloys. *J. Mater. Sci.* **43**, 3009–3027 (2008)
11. Hill, R.: The Mathematical Theory of Plasticity. Oxford University Press, Oxford (1998)
12. Meister, A.: Numerik linearer Gleichungssysteme. Vieweg, Wiesbaden (2007)
13. Roland, M., Kruglova, A., Harste, N., Muecklich, F., Diebels, S.: Numerical Simulation of Al-Si alloys with and without a directional solidification. *Image Anal Stereol* **33**, 29–37 (2014)
14. Saad, Y.: A flexible inner-outer preconditioned GMRES algorithm. *SIAM J. Sci. Comput.* **14**, 461–469 (1993)
15. Saad, Y., Schultz, M.: GMRES: A generalized minimal residual algorithm for solving non-symmetric linear systems. *SIAM J. Sci. Stat. Comput.* **7**, 856–869 (1986)
16. Schenk, O., Gärtner, K.: Solving unsymmetric sparse systems of linear equations with PARDISO. *Journal of Future Generation Computer Systems* **20**(3), 475–487 (2004)
17. Schenk, O., Gärtner, K.: On fast factorization pivoting methods for symmetric indefinite systems. *Elec. Trans. Numer. Anal.* **23**, 158–179 (2006)
18. Shin, S.S., Kim, E.S., Yeom, G.Y., Lee, J.C.: Modification effect of Sr on the microstructures and mechanical properties of Al-10.5Si-2.0Cu recycled alloy for die casting. *Mater. Sci. Eng. A* **532**, 151–157 (2012)
19. Stenzel, O., Hassfeld, H., Thiedmann, R., Koster, L., Oosterhooft, S., van Bavel, S., Wienk, M., Loos, J., Janssen, R., Schmidt, V.: Spatial modelling of the 3D morphology of hybrid polymer-ZnO solar cells, based on electron tomography data. *Annals of Applied Statistics* **5**, 1920–1947 (2011)

-
20. Stenzel, O., Koster, L., Oosterhout, S., Janssen, R., Schmidt, V.: A new approach to model-based simulation of disordered polymer blend solar cells. *Advanced Functional Materials* **22**, 1236–1244 (2012)
 21. Thiedmann, R., Stenzel, O., Spettl, A., Shearing, P., Harris, S., Brandon, N., Schmidt, V.: Stochastic simulation model for the 3D morphology of composite materials in Li-ion batteries. *Computational Materials Science* **50**, 3365–3376 (2011)